Technical University of Denmark

DTU

Microscopic tunneling theory of long Josephson junctions

Grønbech-Jensen, N.; Hattel, Søren A.; Samuelsen, Mogens Rugholm

Link back to DTU Orbit

DTU Library
Technical Information Center of Denmark

Microscopic tunneling theory of long Josephson junctions

N. Grønbech-Jensen*

*Physics Laboratory I, The Technical University of Denmark, DK-2800 Lyngby, Denmark
and Theoretical Division and Advanced Computing Laboratory, Los Alamos National Laboratory, Los Alamos, New Mexico 87545*

S. A. Hattel and M. R. Samuelsen

Physics Laboratory I, The Technical University of Denmark, DK-2800 Lyngby, Denmark

We present a numerical scheme for solving a nonlinear partial integro-differential equation with non-local time dependence. The equation describes the dynamics in a long Josephson junction modeled by use of the microscopic theory for tunneling between superconductors. We demonstrate that the detailed behavior of a solitonic mode (fluxon dynamics) in the junction is different from the results of the conventional perturbed sine-Gordon model.

I. INTRODUCTION

For many years Josephson junctions have been studied successfully using the analogy with the pendulum equation. Similarly, the long Josephson junction (LJJ) has been modeled by the well-known perturbed sine-Gordon equation[1] (PSGE) given by

$$\phi_{xx} - \phi_{tt} - \sin\phi = \alpha\phi_t - \beta\phi_{xxt} - \eta \ . \tag{1}$$

Here ϕ is the phase difference between the quantum-mechanical wave functions of the superconductors defining the junction, the normalized spatial dimension is represented by x, and the time dimension is represented by t, where x and t are normalized to the characteristic Josephson length λ_J and to the inverse plasma frequency ω_p^{-1} of the junction, respectively. The perturbations [right-hand side of Eq. (1)] represent the dissipation and energy input to the system. The tunneling of quasiparticles through the junction is represented by the α term, the surface current of quasiparticles in the superconductors is represented by the β term, and the energy input to the system is the normalized external bias-current density η forced through the junction.

The perturbed sine-Gordon equation has proved itself to explain and predict many characteristics of the LJJ, using different types of perturbations and boundary conditions of the system. In particular, the studies have been focused on the dynamics and manipulation of the so-called first zero field step (ZFS1) in the dc I-V curve, where a localized magnetic-flux quantum travels through the junction. This phenomenon has been explained theoretically by the solitonic 2π-kink solution to the unperturbed sine-Gordon equation (SGE) [left-hand side of Eq. (1)], since the SGE can be integrated to give the exact solution

$$\phi = 4\tan^{-1}\left[\exp\left[\frac{x-ut-x_0}{\sqrt{1-u^2}}\right]\right] \ , \tag{2}$$

where u is the normalized speed of the soliton.

However, in spite of the successful application and qualitative results obtained from the PSGE, the theoretical foundation of this equation is limited to frequency regions much smaller than the gap frequencies of the superconductors—or, in case of different energy gaps of the two superconductors, the validity of PSGE is limited to frequencies much smaller than the difference between the gap frequencies. Strictly speaking, the microscopic theory for tunneling between superconductors predicts that Eq. (1) is only valid for a static field ϕ ($\phi_t = 0$), since no frequency dependence of parameters or information of the gaps of the superconductors are maintained in this model. Recently, LJJ's have been fabricated with very high critical current densities. This results in large plasma frequencies, which again give rise to increased importance of maintaining the information of the gap structure in the model in order to get detailed information. Thus we believe that for many future studies of junctions with high critical current densities, it may prove important to make use of the microscopic theory model instead of the PSGE to explain and predict the detailed behavior of these devices. Also we note that detailed analysis of the real junction is made more direct in the microscopic theory, since all system parameters are fixed by the experimentally measurable quantities: λ_J, ω_p, T, and Δ_i, where T is the temperature of the system and Δ_i is the energy gap of the ith superconductor ($i = 1,2$).

Several other approaches to model small Josephson junctions have been published throughout the years, but none of them seems to be adequate for modeling the dynamics of LJJ's. In Ref. 2 an approach called the successive-approximation method was used to calculate I-V characteristics. The method utilizes the fact that the solution in every single point of the I-V characteristic is strictly periodic with the period $T_p = h/2e\langle V \rangle$. In principle, the same procedure could be used for the calculation of I-V characteristics for the annular LJJ since the voltage in each spatial point is strictly periodic. However, the method is restricted to stationary solutions and offers only little insight into the dynamics of the system, since all calculations are performed in the frequency

domain. In Ref. 3 the whole problem is reformulated into a system of coupled ordinary differential equations, but the necessary approximations seem to be very rough. The electronic device of Ref. 4 used a technique very similar to the one presented in this paper, but the fitting of the current amplitudes seemed to be very inaccurate. In addition to this, the extra effort when coupling a large number of the electronic devices in order to simulate a system with spatial extension seems unreasonable.

II. THE MODEL

Let $\phi(\xi, \tau)$ be the considered phase difference between the two superconductors and let τ and ξ denote the time and space dimension, respectively [τ (sec.), ξ (meter)]. If V is the voltage across the insulator, we have from the well-known Josephson relation that[5]

$$\frac{\partial \phi}{\partial \tau} = \frac{2e}{\hbar} V = \frac{2\pi}{\Phi_0} V, \quad \Phi_0 = \frac{h}{2e} . \tag{3}$$

The tunneling current density at a given space point is given by Refs. 6–10 (here presented in a slight variant of Ref. 7):

$$I(t) = \frac{\Delta_1 + \Delta_2}{eR_n} k \int_{-\infty}^{0} \left[J_p(-kt')\sin\left[\frac{\phi(t) + \phi(t + t')}{2}\right] + \bar{J}_q(-kt')\sin\left[\frac{\phi(t) - \phi(t + t')}{2}\right] \right] dt' + \frac{\hbar \omega_p}{2eR_N}\phi_t . \tag{4}$$

Here the time t is normalized to the inverse plasma frequency ω_p^{-1}, $k = \omega_g / \omega_p$, and the gap frequency is given by $\omega_g = (\Delta_1 + \Delta_2)/\hbar$, where $\Delta_i = \Delta_i(T)$ is the energy gap of the ith superconductor. R_n (Ω m) is the normal resistance above the gap, and the functions J_p and $\bar{J}_q$ are derived from the microscopic theory of tunneling.[8] From this it is well known that the kernel for the quasiparticle current contains a singularity in $\tau = 0$ due to the linear normal resistance. This part is specifically written out in Eq. (4).

The constant k contains information about the relationship between the two characteristic time scales in our system: the plasma frequency and the gap frequency. The latter parameter has no analog in the sine-Gordon (SG) system since any information about the gap is excluded from that description.

We will define the normalized current density J by

$$I(x,t) = I_c J(x,t) , \tag{5}$$

where

$$I_c = \frac{2\Delta}{eR_n} k \int_{-\infty}^{0} J_p(-kt)dt = \frac{2\Delta}{eR_n} \frac{\pi}{4} \tanh\left[\frac{\Delta}{2k_B T}\right] \tag{6}$$

is the usual expression for the critical current. This definition of the critical current makes the normalized super current for static phase differences having its critical value for $J(x,t) = J = 1$, similar to the normally used PSGE normalization of currents giving the supercurrent:

$$I(x,t) = I_c \sin\phi , \quad \phi = \text{const.} \tag{7}$$

We also introduce the normalized space dimension by

$$x = \lambda_J^{-1}\xi, \quad \lambda_J = \sqrt{\phi_0/(2\pi I_c L)} , \tag{8}$$

where $L = \mu_0(2\lambda_L + t_{ox})/W$ with t_{ox} the oxide thickness and W the width of the overlap. In the one-dimensional junction, we assume that $W \ll \lambda_J$.

Finally defining the plasma frequency by

$$\omega_p = \sqrt{2\pi I_c/(\phi_0 C)} , \tag{9}$$

where $C = \epsilon_r \epsilon_0 W/t_{ox}$, we get

$$\phi_{xx} - \phi_{tt} - \bar{J} = \alpha \phi_t - \beta \phi_{xxt} - \eta ,$$

$$\bar{J} = J(x,t) - \alpha \phi_t(x,t) , \tag{10}$$

$$\eta = \frac{I_b}{I_c}, \quad \beta = \frac{\omega_p L}{R} , \quad \alpha = \frac{\hbar \omega_p}{2eR_N I_c} ,$$

where R is the resistance per unit length of the junction describing the transport of quasiparticles in the London layers, and I_b is the bias current density forced through the junction. In making these definitions we have followed the usual procedure for the perturbed sine-Gordon equation as closely as possible (see, e.g., Ref. 11). Equation (10) is then the wave equation modeling the LJJ making use of the microscopic theory for tunneling. As can be seen by comparison with Eq. (1), the modifications to the PSGE are the terms describing the active transport of electrons across the junction. However, the practical solution of this partial integro-differential equation is extremely difficult in its direct form, since the nonlocal time dependence in principle has to be evaluated from $-\infty$ up to the current time in each time step of a numerical integration method. Moreover, the convergence of these integrals [Eq. (4)] is relatively slow, since the kernel functions J_p and J_q approach zero as $1/t$ for large arguments. Thus the direct numerical solution of the above integro-differential equation is in practice impossible.

III. NUMERICAL PROCEDURE

The key point in the numerical procedure is to apply the suggestion made in Ref. 7 to the problem. There the kernel functions are expanded in terms of finite Dirichlet

series:

$$J_p(t) = \text{Re} \left[\sum_{n=1}^{N} \sum_{m=0}^{M} A_{mn}(kt)^m \exp(p_n kt) \right] ,$$

$$\bar{J}_q(t) = \text{Re} \left[\sum_{n=1}^{N} \sum_{m=0}^{M} B_{mn}(kt)^m \exp(p_n kt) \right] ,$$

(11)

where A_{mn}, B_{mn}, and p_n are complex constants and Re( ) means the real part of a complex number. The advantage of this expansion is obviously that the integro part of the wave equation can be updated by considering only the previous time step of a numerical method. Inserting Eq. (11) into the current expression Eq. (4), we find that the tunnel current $J(t)$ at a given space point is given by

$$J(t) = \alpha\phi_t(t) + \frac{1}{\kappa} \left[\sin\frac{\phi(t)}{2} \text{Re} \sum_{\substack{m=0 \\ n=1}}^{N,M} (A_{m,n} + B_{m,n}) \int_{-\infty}^{0} (-t'k)^m e^{-p_n kt'} \cos\frac{\phi(t'+t)}{2} dt' \right.$$

$$\left. + \cos\frac{\phi(t)}{2} \text{Re} \sum_{\substack{m=0 \\ n=1}}^{N,M} (A_{m,n} - B_{m,n}) \int_{-\infty}^{0} (-t'k)^m e^{-p_n kt'} \sin\frac{\phi(t'+t)}{2} dt' \right] ,$$

(12)

where the constants κ and α are

$$\kappa = \text{Re} \left[\sum_{m=0}^{M} \sum_{n=1}^{N} \frac{A_{m,n}}{(-kp_n)^{m+1}} m! \right] , \quad \alpha = \frac{1}{2k^2\kappa} ,$$

(13)

and the critical current density is expressed as

$$I_c = \frac{4\Delta^2}{eR_n\hbar\omega_p}\kappa .$$

(14)

The numerical technique to evolve the solution one step in time is trivial with respect to the phase difference ϕ. Evolving the tunnel current, we have to take the time evolution of the integral into account. We therefore consider the tunnel current at the time $t+dt$:

$$\bar{J}(t+dt) = \frac{1}{\kappa} \left\{ \sin\left[\phi\frac{(t+dt)}{2}\right] \text{Re} \left[\sum_{m,n} (A_{mn} + B_{mn}) \int_{-\infty}^{0} (-t'k)^m e^{-p_n kt'} \cos\left[\frac{\phi(t'+t+dt)}{2}\right] dt' \right] \right.$$

$$\left. + \cos\left[\frac{\phi(t+dt)}{2}\right] \text{Re} \left[\sum_{m,n} (A_{mn} - B_{mn}) \int_{-\infty}^{0} (-t'k)^m e^{-p_n kt'} \sin\left[\frac{\phi(t'+t+dt)}{2}\right] dt' \right] \right\}$$

$$= \frac{1}{\kappa} \left\{ \sin\left[\frac{\phi(t+dt)}{2}\right] \text{Re} \left[\sum_{m,n} (A_{mn} + B_{mn})F_{mn}(t+dt) \right] \right.$$

$$\left. + \cos\left[\frac{\phi(t+dt)}{2}\right] \text{Re} \left[\sum_{m,n} (A_{mn} - B_{mn})G_{mn}(t+dt) \right] \right\} ,$$

(15)

where the functions F, G, f, and g are given by

$$F_{mn}(t) = \int_{-\infty}^{0} (-t'k)^m e^{-kp_n t'} \cos\left[\frac{\phi(t'+t)}{2}\right] dt' ,$$

$$G_{mn}(t) = \int_{-\infty}^{0} (-t'k)^m e^{-kp_n t'} \sin\left[\frac{\phi(t'+t)}{2}\right] dt' ,$$

(16)

$$F_{mn}(t+dt) = e^{kp_n dt} \left[f_{mn}(t,dt) + \sum_{l=0}^{m} \binom{m}{l} (k\,dt)^{m-l} F_{ln}(t) \right] ,$$

(17)

$$G_{mn}(t+dt) = e^{kp_n dt} \left[g_{mn}(t,dt) + \sum_{l=0}^{m} \binom{m}{l} (k\,dt)^{m-l} G_{ln}(t) \right] ,$$

$$f_{mn}(t,dt) = k^m \int_{0}^{dt} (dt-t')^m e^{-kp_n t'} \cos\frac{\phi(t'+t)}{2} dt' ,$$

$$g_{mn}(t,dt) = k^m \int_{0}^{dt} (dt-t')^m e^{-kp_n t'} \sin\frac{\phi(t'+t)}{2} dt' .$$

(18)

Here $F_{mn}(t)$ and $G_{mn}(t)$ are known numbers, since these

contain information only about the past. The functions $f_{mn}(t,dt)$ and $g_{mn}(t,dt)$ are the contributions in order to update $F_{mn}(t)$ and $G_{mn}(t)$ with dt in time.

The problem is now reduced to finding a good estimate of a function [see Eq. (18)]:

$$H_{mn} = \int_0^{dt} (dt-t')^m e^{-p_n kt'} h(t') dt' . \qquad (19)$$

This estimation can be performed in several ways depending on the knowledge we have about the function $h(t')$. If we have access to $h(dt)$, $h(0)$, and $h(-dt)$, as is the case for a finite difference method, we get

$$H_{m,n} = h(dt)\frac{1}{2}\left[\frac{S_{m+2,n}}{(dt)^2} - 3\frac{S_{m+1,n}}{dt} + 2S_{m,n} \right]$$

$$+ h(0)\left[-\frac{S_{m+2,n}}{(dt)^2} + 2\frac{S_{m+1,n}}{dt} \right]$$

$$+ h(-dt)\frac{1}{2}\left[\frac{S_{m+2,n}}{(dt)^2} - \frac{S_{m+1,n}}{dt} \right], \qquad (20)$$

where we have defined

$$S_{m,n} = e^{-kp_n dt}\int_0^{dt} t'^m e^{kp_n t'} dt'$$

$$= e^{-kp_n dt}\frac{m!}{(-kp_n)^{m+1}} - \sum_{l=0}^{m}\frac{m!}{l!}\frac{(dt)^l}{(-kp_n)^{m+1-l}} . \qquad (21)$$

The numerical procedure to solve Eq. (10) is then completed: Evolve $\phi(x,t)$ one time step ahead to $\phi(x,t+dt)$. Find $f_{mn}(t,dt)$ and $g_{mn}(t,dt)$ as sketched above. Update $F_{mn}(t)$ and $G_{mn}(t)$ to the time $t+dt$ and calculate $J(t+dt)$ from Eq. (15).

The computing speed of solving Eq. (10) is much lower than the speed of solving the PSGE. However, we have found, in agreement with Ref. 7, that $N=4,5$ and $M=0$ represents a quite sufficient set of expansion functions to describe the true kernels appropriately. Thus we find that modern work stations are capable of doing simulations of this kind. In fact, our experience is that the most complicated and time-consuming part of the work is to determine the expansion coefficients A_{mn}, B_{mn}, and p_n by fitting to the kernel functions—and not the actual dynamical simulation time.

IV. NUMERICAL RESULTS

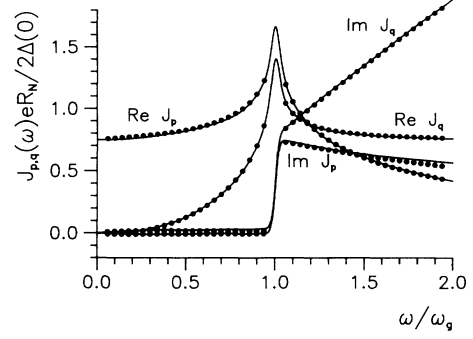We have applied the above sketched numerical procedure to a long (normalized length $L=48$) Josephson

FIG. 1. Fourier transforms of the kernel functions J_p and J_q used in the nonlocal time description. Solid lines are the approximated functions, given by Eq. (11) and Table I. Dots represent the true functions given in, e.g., Ref. 8. These points have been used in the fitting process in order to obtain the approximated functions: $T=4.2$ K and $\Delta=1.35$ meV.

junction with annular geometry in order to study the steady-state wave form of a traveling 2π kink. The numerical scheme for evolving the phase difference $\phi(x,t)$ in time was chosen to a second-order explicit finite difference method, and a fourth- order finite difference method was used to describe the spatial dimension. For simplicity, we have chosen the surface loss term $(\beta\phi_{xxt})$ in the wave equation to be absent. Other system parameters were chosen to be $\Delta_1=\Delta_2=\Delta=1.35$ meV, $T=4.2$ K, $\omega_p=850\times10^9$ rad/sec, describing a high current-density junction of niobium superconductors. We have also tried simulations at higher temperatures, such as $T=0.7T_c=6.4$ K ($\Delta=1.15$ meV). In both cases, we have chosen the normalized time step size to be $dt=0.01$ and the spatial grid size to be $dx=0.02$.

In Tables I and II, we show the chosen expansion coefficients of different temperatures and gaps. In all cases, the choice of $M=0$ has been made. As can be seen from Eq. (18), this makes the numerical procedure faster. In Fig. 1 we show the resulting Fourier transform of the approximated kernel functions (solid curves) together with the analytically given kernels (dots) for $T=4.2$ K and $\Delta(T)=1.35$ meV. The shown dots of the true functions have been used to determine the expansion coefficients of the approximate functions. Clearly, we find that for the case of $T=4.2$ K and $\Delta(T)=1.35$ meV the fitting is very successful. Larger temperatures result in less good agreement between the approximated and the true functions mainly due to a larger smearing of the gap

TABLE I. Expansion coefficients for the Dirichlet series. The choice of $M=0$ and $N=4$ has been made. $T=4.2$ K and $\Delta(T)=1.35$ meV.

n	$\mathrm{Re}(A_{0,n})$	$\mathrm{Im}(A_{0,n})$	$\mathrm{Re}(B_{0,n})$	$\mathrm{Im}(B_{0,n})$	$\mathrm{Re}(p_n)$	$\mathrm{Im}(p_n)$
1	1.262 392	$9.869\,201\times10^{-1}$	$-2.992\,064\times10^{-1}$	$-2.309\,830\times10^{-1}$	$-1.711\,349$	$2.632\,837\times10^{-1}$
2	$3.096\,907\times10^{-1}$	$1.565\,118\times10^{-1}$	$-1.056\,855\times10^{-1}$	$6.310\,330\times10^{-1}$	$-6.597\,119\times10^{-1}$	$7.111\,608\times10^{-1}$
3	$1.309\,572\times10^{-1}$	$1.034\,911\times10^{-2}$	$1.097\,765\times10^{-1}$	$6.287\,742\times10^{-2}$	$-1.778\,335\times10^{-1}$	$9.878\,772\times10^{-1}$
4	$3.785\,244\times10^{-2}$	$8.130\,994\times10^{-4}$	$3.689\,581\times10^{-2}$	$1.407\,315\times10^{-3}$	$-3.432\,953\times10^{-2}$	$1.003\,440$

TABLE II. Expansion coefficients for the Dirichlet series. The choice of $M=0$ and $N=5$ has been made. $T=6.4$ K and $\Delta(T)=1.15$ meV.

n	$\mathrm{Re}(A_{0,n})$	$\mathrm{Im}(A_{0,n})$	$\mathrm{Re}(B_{0,n})$	$\mathrm{Im}(B_{0,n})$	$\mathrm{Re}(p_n)$	$\mathrm{Im}(p_n)$
1	1.1512	2.4884	4.6306	-1.3335	-4.1092	4.6640×10^{-1}
2	4.6448×10^{-1}	-5.3992×10^{-1}	-9.1064×10^{-1}	2.6744	-1.9877	1.6939
3	3.6220×10^{-1}	-2.7513×10^{-2}	2.9323×10^{-1}	5.1136×10^{-1}	-4.9713×10^{-1}	9.7030×10^{-1}
4	1.0081×10^{-2}	6.2859×10^{-3}	7.5897×10^{-2}	3.6630×10^{-3}	-7.4228×10^{-2}	1.0054
5	-1.4238×10^{-2}	-2.0830×10^{-3}	-7.3936×10^{-3}	4.2239×10^{-3}	-4.9681×10^{-2}	9.6522×10^{-1}

singularities in the approximated functions. The success of the approximation of the kernel functions depends, of course, on the patience of the individual who performs the fitting and on the number of expansion parameters available. However, it has been our experience that when restricted to $M=0$ we obtain the best results for the low temperatures. From the plots of the kernel functions, we see the essential difference between the traditional perturbed SG model and the model of microscopic theory, that is to say, the frequency dependence of the coefficients in the perturbed SG model. In Ref. 12 it was found that, in the low-frequency limit, the SG terms are represented as follows: The coefficient to the $\sin\phi$ term is $\mathrm{Re}(I_p)$, $\mathrm{Im}(I_q)$ corresponds to the loss term $\alpha\phi_t$, and $\mathrm{Im}(I_p)$ is the coefficient to a term proportional to $\phi_t\cos\phi$. In the low-frequency limit, $\mathrm{Re}(I_q)$ has no equivalent in the perturbed SG model. The critical current density $\mathrm{Re}(I_p)$ is clearly increasing for increasing frequencies up to the gap frequency, whereafter it is decreasing to zero. The other essential parameter, the quasiparticle loss $\mathrm{Im}(I_q)$, is almost zero for low frequencies and, by an almost steplike behavior at the gap, it is changing to a normal resistance curve. As initial conditions we have made use of the static 2π-kink solution Eq. (2) for $u=0$, since this is an exact solution to Eq. (10), for $\eta=0$. This solution fits very closely to the applied boundary conditions:

$$\phi(0)=\phi(L)-2\pi ,\tag{22}$$

simulating the topological condition of one trapped flux quantum in the annular junction. In addition to the initial condition in ϕ we need an initial condition for the functions F_{mn} and G_{mn}. Using the fact that we have chosen a static solution as initial condition for the phase difference, we easily get from Eq. (16) that

$$F_{mn}(x,0)=\frac{m!}{k(-p_n)^{m+1}}\cos\left[\frac{\phi(x,0)}{2}\right] ,$$
$$G_{mn}(x,0)=\frac{m!}{k(-p_n)^{m+1}}\sin\left[\frac{\phi(x,0)}{2}\right] .\tag{23}$$

We here note that the numerical procedure is not very sensitive to the initial conditions in F_{mn} and G_{mn}. We have used, without any complications, the initial conditions Eq. (23) even for nonstatistic initial conditions in ϕ.

In Fig. 2 we show the normalized bias-velocity (I-V) curves of different temperatures. For these numerical experiments, the initial conditions Eq. (23) have been used to a system with no bias current ($\eta=0$) and for a system

length of $L=48$ in order to simulate an infinite system length. The bias current η was increased in small steps $\delta\eta$, after each step allowing the system to relax in 1000 normalized time units before measuring the steady-state speed of the soliton (voltage across the junction). The speed (u) is found by measuring the increase of the average phase difference in 100 normalized time units, giving the normalized voltage. The velocity of the solitonic wave is then given by $u=VL/2\pi$.

In Fig. 2 one-soliton curves are calculated by use of the step size $\delta\eta=10^{-2}$ (dashed lines, right axis) and $\delta\eta=10^{-3}$ (solid lines, left axis). The upper dashed and solid curves are for $T=6.4$ K and the lower dashed and solid curves are for $T=4.2$ K. Clearly, the soliton velocity is larger for lower temperatures than for larger, which of course is to be expected. The abrupt jumps of the voltage represented by horizontal lines from the top of the dashed curves are due to the disappearance of the localized 2π-kink structure, which becomes unstable into a mode characterized by almost homogeneously distributed magnetic flux and voltage. Actually the junction changes from a mode determined by the plasma frequency into a mode determined by the gap frequency. This happens for η values significantly smaller than $\eta=1$, and it seems to happen for even smaller bias values for lower temperatures than for the higher temperatures. This characteristic is different from the conventional SG model, where the localized SG kink may exist in an infinite-length system for all $|\eta|<1$ if the surface loss is absent ($\beta=0$).[13] The reason for the instability of the kink in the strongly driven system with no surface loss is found in Fig. 3. Here, we have plotted an instantaneous picture of the x
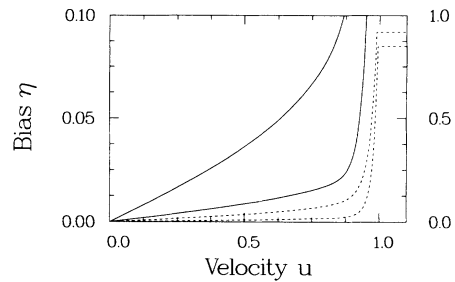

FIG. 2. Bias speed curve (I-V curve) for the system length $L=48$, with a step size $d\eta=10^{-3}$ (solid lines, left axis) and $d\eta=10^{-2}$ (dashed lines, right axis). Upper solid and dashed curves are for the case $T=6.4$ K, and the lower curves for $T=4.2$ K.
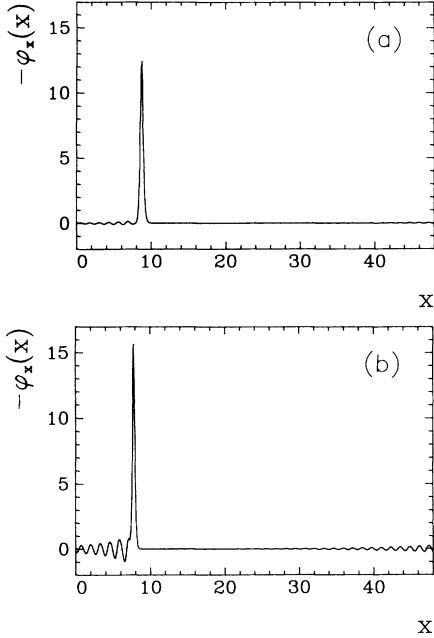
FIG. 3. Magnetic-flux density ϕ_x as a function of space in a steady-state motion for the bias values (a) $\eta=0.5$ and (b) $\eta=0.8$. $T=4.2$ K.

derivative of the steady-state ϕ field for different values of the bias-current density η and $T=4.2$ K. In Fig. 3(a) we show the profile for a value of $\eta=0.5$, and for $\eta=0.8$ in Fig. 3(b). For higher temperatures (not presented in the figures) the soliton profiles are broader, and the velocity is smaller than for the lower temperatures due to the higher effective damping. This is of course in analogy with the Lorentz contraction in the unperturbed SG system, where the fast profile is narrow compared to the slow profile. Likewise, larger η values result in a more narrow steady-state profile, but what is more interesting is that the traveling soliton is followed by an oscillating tail, giving rise to radiative losses. Comparing Fig. 3(a) for $\eta=0.5$ to Fig. 3(b) for $\eta=0.8$, we find that the amplitude of these damped oscillations increases as η is increased. This is quite similar to the behavior of the kink in the perturbed SG model with surface losses, since that system also shows a steady-state traveling wave followed by an oscillating tail.[13,14] However, the oscillation frequency is quite different, since the SG system can provide the plasma frequencies only, while the microscopic theory also provides the gap frequency as a characteristics frequency in the system. The gap frequency is shown[15] to be exited locally in the system, if a step in the phase difference takes place. Since a moving kink profile acts as a step function in a given point of the junction, we expect an oscillating tail with the frequency $\omega=\omega_g=2\Delta(T)/\hbar$ in time and the wave number $k=2\pi/\lambda=\omega_g/u$, where u is the velocity of the traveling wave. In normalized units, we get for the specific choices of parameters made here

$$T=4.2 \text{ K}: \quad \omega_g=4.85, \quad \lambda=u\times1.30\approx1.29,$$
$$T=6.4 \text{ K}: \quad \omega_g=4.13, \quad \lambda=u\times1.52\approx1.49 . \tag{24}$$

In comparison, we have measured the wavelengths for $\eta=0.8$ to be

$$T=4.2 \text{ K}: \quad \lambda\approx1.28,$$
$$T=6.4 \text{ K}: \quad \lambda\approx1.47 , \tag{25}$$

which is in quite good agreement with the predicted wavelength.

Thus we conclude that the fast moving soliton does in fact suffer from radiative losses at the gap frequency $\omega_g=2\Delta/\hbar$. We note here that the treatment of Ref. 15 predicts that a step function with the weight of exactly $2\pi n$ should not give rise to any exitation of the gap frequency. This is of course disappointing from the point of view of 2π kinks, but we should here keep in mind that the kink is not a perfect step function and it should in this relation be treated as a more complicated wave form. We should also note that, for the specific values of parameters used here, the gap frequencies for $T=4.2$ K and $T=6.4$ K are very close to the frequencies of the linear Klein-Gordon modes $\omega=\sqrt{1+k^2}$. However, we observe that the measured spatial wavelength λ scales with the energy gap, which strongly indicates that this phenomenon is due to the gap structure in the local tunneling processes, and not the spatial wave dynamics.

An interesting consequence of the radiative losses is that it may provide a spatially harmonical potential for a second soliton, and hereby create stable states of several bunched solitons. We now consider the system containing two solitons with the internal distances δ. If we assume that the soliton wave profiles to be very narrow, we do not expect that any significant repulsion is taking place between the two 2π-kinks, provided that we do not choose δ too small. However, as seen from Figs. 3, the radiation is spatially of long range. Assuming that the oscillations are exponentially damped, that the frequency is indeed the gap frequency, and that the soliton profile is smaller than the spatial wavelength of the radiation, we can approximate an interaction energy H_I between a soliton and the radiation by
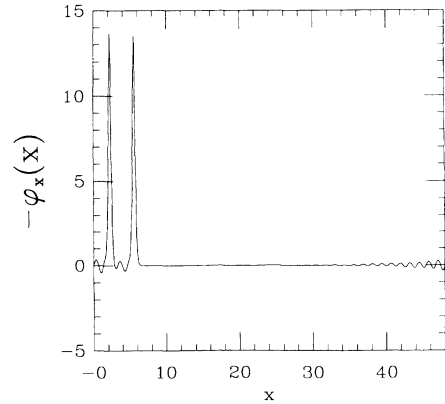

FIG. 4. Magnetic-flux density ϕ_x as a function of space in a steady-state motion of two magnetic-flux quanta in the annular system for $\eta=0.6$ with an initial distance between the magnetic-flux quanta of $\delta_0=3.25$.
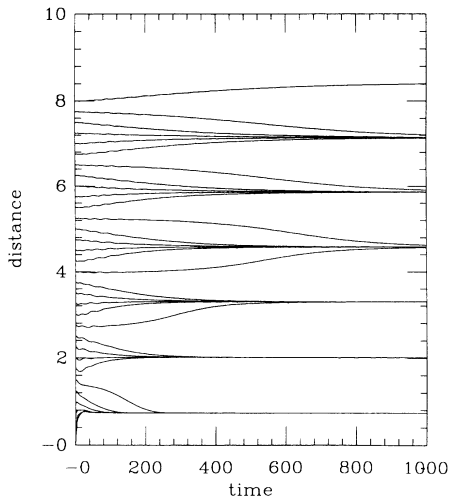
FIG. 5. Distance between two magnetic-flux quanta as a function of time: $T = 4.2$ K, $\omega_p = 850 \times 10^9$ rad/sec, and $\eta = 0.6$.

$$H_I(\delta) = ae^{-(\epsilon+\delta)\bar{\alpha}}\cos[(\epsilon+\delta)k] , \qquad (26)$$

where α is some unknown amplitude, δ is the distance between the two solitons, ϵ is a phase factor denoting the internal phase between a kink and its radiation, and k is the wave number corresponding to the steady-state velocity and energy gap: $k = \omega_g/u$. From this, we can then predict multistable bunched soliton states characterized by the internal distances

$$\delta_* = (\pi + 2\pi p)1/k - \epsilon , \quad p = 1, 2, \ldots . \qquad (27)$$

That is, the internal distance of a bound state of two kinks is quantized according to the gap frequency and the velocity of the steady state. In order to check this prediction, we have performed numerical experiments, with two 2π kinks as initial conditions. In Fig. 4, we have shown the final steady state, obtained after 1000 normalized time units, for the bias value $\eta = 0.6$ and an initial internal distance of $\delta_0 = 3.25$. We have found that many different states can be obtained depending on the initial distance δ_0 between the kinks. All these simulations were performed for the temperature $T = 4.2$ K. In Fig. 5 we illustrate the quantized steady-state distance by showing the time evolution of the distance for different values of the initial distance and $\eta = 0.6$. From this plot, it is evident that the steady-state internal distance is quantized

and, further, the spacing between the final distances is almost constant and equal to the predicted wavelength of the traveling gap oscillation Eq. (27). We have found a similar picture for values of η ranging from 0.2 to 0.6. What is also an interesting information from this plot is that the relaxation time toward the steady state increases as the initial distance increases. From this, one may calculate the decay factor $\bar{\alpha}$ in Eq. (26).

V. DISCUSSION

We have applied the method of expanding the kernel functions in the Dirichlet series and, from this, were able to do simulations of LJJ's described by the microscopic theory. A detailed description of the numerical procedure is shown, and some specific expansion parameters are given for experimentally realistic sets of temperatures and energy gaps of the superconductors. In order to test the numerical procedure, we have applied the method to a long annular system, simulating an infinite length. It is found that a kink suffers from radiative losses at the gap frequency, when it is forced to move with large velocities. These losses, visible as a tail of radiation after the soliton, also cause the localized solitonic mode to switch out to the nonlocalized rotating mode, which is a quite similar behavior to the SG system perturbed with surface losses.[13,14] In analogy with the SG system perturbed with the surface losses, we have observed bunched states of solitons, and the possible internal distances between two solitons were found to be quantized in accordance with the spatial wavelength of the radiative tail of the solitons. We note that most experimental systems are relatively short in normalized length and have open boundary conditions, so our numerical studies here may not be directly applicable to experiments. However, our aim in this paper has mainly been to develop a numerical procedure to make progress to the study of this very complicated model. Long Josephson junctions are now fabricated[16] with very high critical current densities, resulting in plasma frequencies of $\omega_p \approx 1.3 \times 10^{12}$ rad/sec. For these junctions, we expect that the nonlocal time dependence as well as the frequency dependence of parameters will prove to be important. In particular, the solitonic mode of a traveling kink contains a broad range of frequency components, which may be affected by the gap structure of the tunneling process. We hope in the near future to be able to do direct quantitative comparisons between the results of our numerical scheme and experiments made on real LJJ's of high critical current densities.

*Present address: Department of Applied Physics, Stanford University, Stanford, California 94305.
[1]See, e.g., A. Barone and G. Paterno, *Physics and Applications of the Josephson Effect* (Wiley, New York, 1982).
[2]D. G. McDonald, E. G. Johnson, and R. E. Harris, Phys. Rev. B **13**, 1028 (1976).
[3]S. N. Erné and H. Lübbig, J. Appl. Phys. **51**, 4927 (1980).
[4]Daniel G. Jablonski, J. Appl. Phys. **53**, 7458 (1982).

[5]B. D. Josephson, Phys. Lett. **1**, 251 (1962).
[6]L.-E. Hasselberg, M. T. Levinsen, and M. R. Samuelsen, Phys. Rev. B **9**, 3757 (1974).
[7]A. A. Odintsov, V. K. Semenov, and A. B. Zorin, IEEE Trans. Magn. **MAG-23**, 763 (1986).
[8]N. R. Werthamer, Phys. Rev. **147**, 255 (1966).
[9]U. K. Poulsen, Ph.D. thesis, The Technical University of Denmark, 1973 (unpublished).

[10]Richard E. Harris, Phys. Rev. B **10**, 84 (1974).

[11]P. S. Lomdahl, Ph.D. thesis, The Technical University of Denmark, 1982 (unpublished).

[12]Richard E. Harris, Phys. Rev. B **11**, 3329 (1975).

[13]S. Pagano, M. P. Sørensen, P. L. Christiansen, and R. D. Par-mentier, Phys. Rev. B **38**, 4677 (1988).

[14]S. Pagano, Ph.D. thesis, The Technical University of Denmark, 1987 (unpublished).

[15]Richard E. Harris, Phys. Rev. B **13**, 3818 (1976).

[16]A. Davidson (private communication).